33RD CONGRESS
OF THE INTERNATIONAL COUNCIL
OF THE AERONAUTICAL SCIENCES
STOCKHOLM, SWEDEN, 4-9 SEPTEMBER, 2022

ICAS 2022 SWEDEN

STUDY OF THE IMPACT OF AZIMUTHAL FLOW DISTORTION ON IN-DUCT ACOUSTIC PROPAGATION USING A MULTIMODAL FORMULATION

B. Mangin[1], M. Daroukh[1] & G. Gabard[2]

[1]DAAA, ONERA, Université Paris Saclay, F-92322 Châtillon, France
[2]Laboratoire d'Acoustique de l'Université du Mans (LAUM), UMR 6613, Institut d'Acoustique - Graduate School (IA-GS), CNRS, Le Mans Université, France

Abstract

The evolution of aircraft engines towards Ultra High Bypass Ratio (UHBR) architectures goes with a shortening of the nacelle length responsible for an important circumferential inhomogeneity of the flow, called distortion, inside the inlet duct. This distortion is also expected to be even more pronounced in new integration concepts with Boundary Layer Ingestion (BLI) because of the important asymmetry of the geometry. Numerical studies have already shown that such distortion can significantly impact the acoustic propagation inside the nacelle and, consequently, the sound radiated by the engine. This paper presents a fast and accurate multimodal method applicable to the computation of the acoustic field in such distorted flow, provided that it remains potential. This is achieved by transforming the original three-dimensional set of equations into a one-dimensional problem using the Fourier transform of the sound disturbances in the azimuthal direction and a projection on shifted Chebyshev polynomials in the radial direction. The formulation is verified against a numerical finite-difference solution and is shown to give consistent results for modes propagating in distorted flows.

Keywords: Duct acoustics, multimodal method, flow distortion

1. Introduction

In modern aero-engines, the nacelle is designed so that the flow is uniform during straight and level cruise flights (with low angle of incidence) to maximize engine efficiency. Nevertheless, the plane is under high incidence during landing or takeoff operations, which implies that the engine axis and the external flow are not aligned. Consequently, the flow that enters the engine is no longer axisymmetric, as illustrated in figure 1. The air inlet attenuates this inhomogeneity, and the distortion levels tend to decrease sharply. Therefore, this distortion can be considered negligible almost everywhere for long air-inlets, and the interaction of this distortion with the acoustics can be neglected. However, the air-inlet length tends to be shortened for new engine geometries, and part of this conditioning effect is lost. Typically for Ultra High Bypass Ratio (UHBR) engines, high azimuthal distortions are expected in the most significant part of the air inlet [1].

Such a distortion can significantly impact the acoustics, and classical propagation models [2], which consider that the mean flow is axisymmetric, cannot be used anymore. New methodologies are needed. A first study done by Sofrin & Cicon [3] has been carried out to understand the consequence of such a phenomenon on the acoustic field. Using an eigenanalysis on a simplified propagation equation, they showed that the uniform flow modes become distorted and that new modes need to be introduced to represent the acoustics.

Other studies followed the idea presented by Sofrin & Cicon and extended it. Astley *et al.* [4] solved the exact propagation equation, the Pridmore-Brown equation, using an eigenanalysis in the case of a duct of constant radius. Comparisons with results of a real aero-engine inlet, for which an experimental azimuthal breakdown of the measured sound pressure is available, proved this method to be

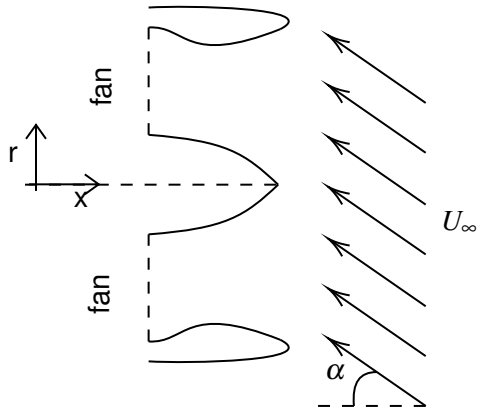

Figure 1 – An engine inlet with an incoming flow of incidence α.

an accurate prediction tool. They have also shown a weak coupling between the hydrodynamic and acoustic modes for low levels of flow distortion. This eigenanalysis can also be applied to flows with a high level of inhomogeneity in ducts of varying radius by using a two-way sweep calculation [5]. This method offers good results, but the associated computational cost is high and does not appear to be of significant interest compared to numerical methods [1, 6]. One element that slows down the calculation is the need to propagate the hydrodynamic modes, the wavelengths of which are small compared to the characteristic acoustic wavelengths. Ignoring the hydrodynamics would imply a significant gain in terms of central processing unit (CPU) cost by reducing the needed axial discretization and the number of variables to compute. To that extent, Guérin *et al.* [7] made an approximation for turbo-engines that seemed to give consistent results by considering that the flow was potential. Several studies based on finite element methods (FEM) use that approximation to compute the acoustic field when a distorted potential flow is assumed [8, 9]. They offer results of main interest, but the CPU cost for such computation is still significant. The current paper's idea is to reduce the calculation time again by taking advantage of the core ducted aspect of the problem to distinguish the axial resolution from the transverse one (modal representation).

This idea is the basis of the multimodal method (MM), which consists in rearranging the acoustic problem in a set of coupled one-dimensional (1D) amplitude equations describing the evolution of the modes. This method is generally used to calculate propagation inside ducts without flow [10, 11, 12, 13, 14] but it has recently been extended cases with simplified two dimensional potential flows [15]. In classic multimodal formulation, the acoustic variables are projected on the local transverse eigenmodes, composed of separable functions in the radial and azimuthal directions (Fourier decomposition in the azimuthal direction, Bessel decomposition in the radial direction). This basis cannot be kept in a duct with a distorted flow since no separable functions can be obtained. Nevertheless, a Fourier transform of the acoustic variables can still be done in the azimuthal direction since, in most cases, the flow is not far from being axisymmetric [4]. Therefore the circumferential Fourier spectrum is finite and limited to the nearest azimuthal orders. In the radial direction, a basis composed of Chebyshev polynomials is used since its offers excellent convergence priorities [15].

The paper is set as follows. A description of the developed multimodal method with distorted potential flows is fisrt given in section 2 . In section 3 , the method is validated and the effects of inflow distortion are highlighted by comparison with cases without distortion. Conclusions and discussions are finally provided in section 4 .

2. Multimodal formulation with distorted potential flow

2.1 Model assumptions

The domain considered for the acoustic resolution is the air-inlet of an aero-engine during landing or takeoff operations. The nacelle is approximated by an axisymmetric duct. The viscous effects are neglected and no-shock is expected. Taking all these considerations into account, the flow is considered as a perfect isentropic subsonic compressible gas flow.

In the following, all the parameters are transformed to be dimensionless: densities are normalized

by a reference density ρ_∞, velocities are normalized by a reference sound speed c_∞, spatial dimensions by the typical duct radius R_∞, velocity potentials by $R_\infty c_\infty$, and pressures by $\rho_\infty c_\infty^2$. We begin by considering an associated cylindrical coordinate system (x,r,θ), with the associated eigenvectors $(\mathbf{e}_x,\mathbf{e}_r,\mathbf{e}_\theta)$. The hub and tip radius are written R_1 and R_2 respectively. The analysis is done in the frequency domain and the characteristic pulsation of the source $\omega = 2\pi f$ is introduced, with f the frequency. The velocity vector, the density, the speed of sound and the pressure variables are written: $\tilde{\mathbf{v}} = \mathbf{V} + \mathrm{Re}(\mathbf{v}\ \mathrm{e}^{i\omega t}) = (U,V,W) + \mathrm{Re}((u,v,w)\ \mathrm{e}^{i\omega t})$, $\tilde{\rho} = D + \mathrm{Re}(\rho\ \mathrm{e}^{i\omega t})$, $\tilde{c} = C + \mathrm{Re}(c\ \mathrm{e}^{i\omega t})$, $\tilde{p} = P + \mathrm{Re}(p\ \mathrm{e}^{i\omega t})$ respectively. The capital letters denote the time-averaged values, and the lower-case letters represent the unsteady harmonic perturbations. The notations are identical to those used by Cooper & Peake [16].
In this framework, the steady Euler equations are:

$$\begin{aligned} \nabla\cdot(D\mathbf{V}) &= 0, \\ D(\mathbf{V}\cdot\nabla)\mathbf{V} &= -\nabla P, \\ C^2 = \frac{\gamma P}{D} &= D^{\gamma-1}, \end{aligned} \tag{1}$$

where γ is the ratio of specific heats.
For the unsteady harmonic perturbations, the perturbation velocity is decomposed into a rotational and an irrotational term: $\mathbf{v} = \mathbf{v}^R + \nabla\phi = (u_x^R, u_r^R, u_\theta^R) + \nabla\phi$, with ϕ the velocity potential and $\nabla.\mathbf{v}^R = 0$. By imposing that the unsteady pressure only depends on the acoustic potential $p = -D\ \mathrm{D}\phi/\mathrm{D}t$, the linearized Euler equations (LEE) for the perturbation variables can be written as follows[16]:

$$\begin{aligned} \nabla\cdot(D\nabla\phi) - D(i\omega + \mathbf{V}\cdot\nabla)\left[\frac{1}{C^2}(i\omega+\mathbf{V}\cdot\nabla)\phi\right] &= \nabla\cdot(D\mathbf{v}^R), \\ (i\omega+\mathbf{V}\cdot\nabla)\mathbf{v}^R + (\mathbf{v}^R\cdot\nabla)\mathbf{V} &= -\xi\times\nabla\phi, \end{aligned} \tag{2}$$

with $xi = rot(V)$ is the mean vorticity.
The potential part of the velocity follows a wave equation, whereas the rotational part follows a transport equation. Therefore, the first part can be associated with acoustic propagation, when the second can be associated with hydrodynamic convection. The two equations are coupled by the mean vorticity xi. When this term is equal to zero, an apparent dissociation between both equations is obtained, and the acoustic problem reduces to the resolution of the equation:

$$\nabla\cdot(D\nabla\phi) - D(i\omega+\mathbf{V}\cdot\nabla)\left[\frac{1}{C^2}(i\omega+\mathbf{V}\cdot\nabla)\phi\right] = 0. \tag{3}$$

For the following of the paper, the flow is considered potential (i.e. $xi = 0$) and this last equation is solved. The fact that the flow is potential implies that:

$$\frac{\partial W}{\partial x} = \frac{1}{r}\frac{\partial U}{\partial\theta}, \quad \frac{1}{r}\frac{\partial rW}{\partial r} = \frac{1}{r}\frac{\partial V}{\partial\theta}, \quad \frac{\partial U}{\partial r} = \frac{\partial V}{\partial x}. \tag{4}$$

Note that if the flow is distorted, the term $\partial U/\partial\theta$ is not equal to zero; therefore, the term $\partial W/\partial x$ is also non zero. This means that the distortion causes an axial variation of the mean flow.

2.2 Modified wave equation

The multimodal formulation for a simplified potential flow has already been studied in [15]. As in the latter study, the formulation is written using the acoustic velocity potential ϕ and it axial derivative, $q = \frac{\partial\phi}{\partial x}$. The acoustic variables are projected on transverse cross-section modes such that the problem can be written as a set of first-order coupled differential equations. This basis is denoted here $(\varphi_j)_{j\in\mathbb{N}}$. As an example, the acoustic potential writes: $\phi = \sum_j \phi_j(x)\varphi_j(x,r,\theta)$. Equation (3) is multiplied by a test function φ_i^*, chosen to be the complex conjugate of a basis function, and is integrated over a duct transverse surface S. Then by applying the divergence theorem, and after some manipulation with the mean flow mass conservation equation, we obtain:

$$\begin{aligned}
&\frac{\mathrm{d}}{\mathrm{d}x}\left(\int_S D(1-M_x^2)q\varphi_i^*\mathrm{d}S\right)-\frac{\mathrm{d}}{\mathrm{d}x}\left(\int_S DU\varphi_i^*\frac{1}{C^2}\frac{\mathrm{D}_\perp\phi}{\mathrm{D}t}\mathrm{d}S\right)=\int_S D(1-M_x^2)q\frac{\partial\varphi_i^*}{\partial x}+D\nabla_\perp\varphi_i^*.\nabla_\perp\phi\\
&\quad-\frac{D}{C^2}\left(V^2\frac{\partial\phi}{\partial r}\frac{\partial\varphi_i^*}{\partial r}+\left(\frac{W}{r}\right)^2\frac{\partial\phi}{\partial r}\frac{\partial\varphi_i^*}{\partial r}+w^2\phi\varphi_i^*+UV\left(\frac{\partial\varphi_i^*}{\partial r}\frac{\partial\phi}{\partial x}+\frac{\partial\phi}{\partial r}\frac{\partial\varphi_i^*}{\partial x}\right)\right.\\
&\quad+\frac{UW}{r}\left(\frac{\partial\varphi_i^*}{\partial\theta}\frac{\partial\phi}{\partial x}+\frac{\partial\phi}{\partial\theta}\frac{\partial\varphi_i^*}{\partial x}\right)+\frac{WV}{r}\left(\frac{\partial\varphi_i^*}{\partial r}\frac{\partial\phi}{\partial\theta}+\frac{\partial\phi}{\partial r}\frac{\partial\varphi_i^*}{\partial\theta}\right)\\
&\left.+\mathrm{i}U\omega\left(\phi\frac{\partial\varphi_i^*}{\partial x}-\frac{\partial\phi}{\partial x}\varphi_i^*\right)+\mathrm{i}V\omega\left(\phi\frac{\partial\varphi_i^*}{\partial r}-\frac{\partial\phi}{\partial r}\varphi_i^*\right)+\mathrm{i}\frac{W}{r}\omega\left(\phi\frac{\partial\varphi_i^*}{\partial\theta}-\frac{\partial\phi}{\partial\theta}\varphi_i^*\right)\right)\mathrm{d}S,
\end{aligned}\tag{5}$$

where $\dfrac{\mathrm{D}_\perp\phi}{\mathrm{D}t}=\mathrm{i}\omega\phi+V\dfrac{\partial\phi}{\partial r}+\dfrac{W}{r}\dfrac{\partial\phi}{\partial\theta}$ is the transverse convective derivative, and $M_x=U/C$ is the axial Mach number.

The acoustic variables are decomposed on the transverse basis to obtain the multimodal equation to be solved:

$$\begin{aligned}
&\left(\int_S D(1-M_x^2)\varphi_j\varphi_i^*\mathrm{d}S\right)\frac{\mathrm{d}q_n}{\mathrm{d}x}-\left(\int_S\frac{DU}{C^2}\left(\varphi_i^*\frac{\mathrm{D}_\perp\varphi_j}{\mathrm{D}t}-\varphi_j\frac{\mathrm{D}_\perp\varphi_i^*}{\mathrm{D}t}\right)\mathrm{d}S\right)\frac{\mathrm{d}\phi_n}{\mathrm{d}x}-\frac{\mathrm{d}}{\mathrm{d}x}\left(\int_S\frac{DU}{C^2}\varphi_i^*\frac{\mathrm{D}_\perp\varphi_j}{\mathrm{D}t}\mathrm{d}S\right)\phi_n=\\
&\quad-\frac{\mathrm{d}}{\mathrm{d}x}\left(\int_S D(1-M_x^2)\varphi_j\varphi_i^*\mathrm{d}S\right)q_n+\int_S D(1-M_x^2)\varphi_j\frac{\partial\varphi_i^*}{\partial x}q_n+D\nabla_\perp\varphi_i^*.\nabla_\perp\varphi_j\\
&\quad-\frac{D}{C^2}\left(\frac{\mathrm{D}_\perp\varphi_j}{\mathrm{D}t}\frac{\mathrm{D}_\perp\varphi_i^*}{\mathrm{D}t}+U\left(\frac{\partial\varphi_j}{\partial x}\frac{\mathrm{D}_\perp\varphi_i^*}{\mathrm{D}t}+\frac{\mathrm{D}_\perp\varphi_j}{\mathrm{D}t}\frac{\partial\varphi_i^*}{\partial x}\right)\right)\mathrm{d}S\phi_n.
\end{aligned}\tag{6}$$

This last equation can be rearranged in the following matrix form:

$$\begin{pmatrix}\mathscr{A}_{11}&0\\\mathscr{A}_{21}&\mathscr{A}_{22}\end{pmatrix}\frac{\mathrm{d}}{\mathrm{d}x}\begin{pmatrix}\phi_n\\q_n\end{pmatrix}=\begin{pmatrix}\mathscr{M}_{11}&\mathscr{M}_{12}\\\mathscr{M}_{21}&\mathscr{M}_{22}\end{pmatrix}\begin{pmatrix}\phi_n\\q_n\end{pmatrix},\tag{7}$$

with:

$$\begin{aligned}
\mathscr{A}_{11}&=\mathscr{A}_{22}=\mathscr{M}_{12}=\int_S D(1-M_x^2)\varphi_j\varphi_i^*\mathrm{d}S,\\
\mathscr{M}_{11}&=-\int_S D(1-M_x^2)\varphi_j\frac{\partial\varphi_i^*}{\partial x}\mathrm{d}S,\\
\mathscr{A}_{21}&=-\int_S\frac{DU}{C^2}\left(\varphi_i^*\frac{\mathrm{D}_\perp\varphi_j}{\mathrm{D}t}-\varphi_j\frac{\mathrm{D}_\perp\varphi_i^*}{\mathrm{D}t}\right)\mathrm{d}S,\\
\mathscr{M}_{21}&=\int_S D\nabla_\perp\varphi_i^*.\nabla_\perp\varphi_j-\frac{D}{C^2}\left(\frac{\mathrm{D}_\perp\varphi_j}{\mathrm{D}t}\frac{\mathrm{D}_\perp\varphi_i^*}{\mathrm{D}t}+U\left(\frac{\partial\varphi_j}{\partial x}\frac{\mathrm{D}_\perp\varphi_i^*}{\mathrm{D}t}+\frac{\mathrm{D}_\perp\varphi_j}{\mathrm{D}t}\frac{\partial\varphi_i^*}{\partial x}\right)\right)\mathrm{d}S\\
&\quad+\frac{\mathrm{d}}{\mathrm{d}x}\left(\int_S\frac{DU}{C^2}\varphi_i^*\frac{\mathrm{D}_\perp\varphi_j}{\mathrm{D}t}\mathrm{d}S\right),\\
\mathscr{M}_{22}&=-\frac{\mathrm{d}}{\mathrm{d}x}\left(\int_S D(1-M_x^2)\varphi_j\varphi_i^*\mathrm{d}S\right)+\int_S D(1-M_x^2)\varphi_j\frac{\partial\varphi_i^*}{\partial x}\mathrm{d}S.
\end{aligned}\tag{8}$$

2.3 Axial integration and boundary conditions

Equation (7) is unstable and cannot be integrated directly because of evanescent modes [12]. The multimodal method allows to solve this issue by defining an admittance matrix Y such that $q_n(x)=Y(x)\phi_n(x)$. This admittance links the potential and its derivative and is therefore characteristic of the reflection and refraction index of the medium (Poincaré–Steklov operator). A new stable equation, called the Riccati equation, is obtained for this matrix:

$$\frac{\mathrm{d}Y}{\mathrm{d}x}=-Y\mathscr{A}_{11}^{-1}\mathscr{M}_{11}-Y\mathscr{A}_{11}^{-1}\mathscr{M}_{12}Y+\mathscr{A}_{22}^{-1}\mathscr{M}_{21}-\mathscr{A}_{21}\mathscr{A}_{11}^{-1}\mathscr{M}_{11}+(\mathscr{A}_{22}^{-1}\mathscr{M}_{22}-\mathscr{A}_{21}\mathscr{A}_{11}^{-1}\mathscr{M}_{12})Y,\tag{9}$$

and is solved using a Magnus-Moebius scheme [17, 12].

The solving allows assessing the admittance value inside the duct given an initial value Y_e, called the radiation condition. Generally, the admittance is defined as a fixed point of the Riccati equation in multimodal methods. These points solve the equation when all the global variables do not vary axially, which generally corresponds to extending the duct into an infinite uniform duct. However, extending the duct and keeping the potential flow hypothesis necessarily implies axially varying flow variables in the presence of distortion (see section 2.1). In order to have non-varying global variables here, the duct is extended and the distortion is artificially kept constant. This violates the potential flow hypothesis, but this allows to derive a quasi non-reflecting boundary condition on the artificial boundary.
A local transverse eigenvalue problem is defined at the exit plane to get as close as possible to the usual constant duct radiation condition. The solution is written using a summation of local transverse modes over the cross-section that locally propagate or decay exponentially with the axial distance:

$$\begin{pmatrix} \phi_n(x) \\ q_n(x) \end{pmatrix} = \sum_i \alpha_i \begin{pmatrix} w_{i1} \\ w_{i2} \end{pmatrix} e^{\mathrm{i}\lambda_i x}, \tag{10}$$

where $w_{i1/2}$ are eigenvectors representing the weight associated with the distribution over the cross-sectional basis functions φ_i, λ_i are the associated axial wavenumbers and α_i are constants. By injecting the expression (10) into the propagation equation (7), and by using the basis properties of the eigenvectors, the following eigenvalue problem is obtained:

$$\mathrm{i}\lambda_i \begin{pmatrix} \mathscr{A}_{11} & 0 \\ \mathscr{A}_{21} & \mathscr{A}_{22} \end{pmatrix} \begin{pmatrix} w_{i1} \\ w_{i2} \end{pmatrix} = \begin{pmatrix} \mathscr{M}_{11} & \mathscr{M}_{12} \\ \mathscr{M}_{21} & \mathscr{M}_{22} \end{pmatrix} \begin{pmatrix} w_{i1} \\ w_{i2} \end{pmatrix}. \tag{11}$$

Here, the solution is split into forward and backward waves based on the quadrants of the imaginary plane in which their associate eigenvalue lies. This allows, for example, to construct the forward matrix $\begin{pmatrix} \phi_{n+} \\ q_{n+} \end{pmatrix} \propto \begin{pmatrix} W_{1+} \\ W_{2+} \end{pmatrix} e^{\Lambda_+ x}$ with $\begin{pmatrix} W_{1+} \\ W_{2+} \end{pmatrix} = \begin{pmatrix} w_{11},...,w_{n1} \\ w_{12},...,w_{n2} \end{pmatrix}$ and $\Lambda_+ = diagonal(i\lambda_1,...,i\lambda_n)$ and where $\lambda_1,...,\lambda_n$ and $w_{11/2},...,w_{n1/2}$ are the eigenvalues and eigenvectors associated to forward waves. The backward Y_- and forward Y_+ admittances are introduced, and link the backward and forward modes respectively: $q_{n+} = Y_+ \phi_{n+}$, $q_{n-} = Y_- \phi_{n-}$.
At the end of the duct, the waves only propagate forwards ($Y_e = Y_+$). The expression of the admittance matrix is then straightforward at the duct exit and writes:

$$Y_e = W_{2+} W_{1+}^{-1} = W_{1+} \Lambda_+ W_{1+}^{-1}. \tag{12}$$

This boundary condition is usually imperfect since the radiation condition is a jump in the model from a potential to a non-potential flow. Therefore, this could create artificial reflections, but this phenomenon is expected to be limited. Let us mention that contrary to the case of a uniform fluid in a constant duct, the study of the modal problem in the presence of a mean flow still raises many open mathematical questions [18].

2.4 Injection of a mode

The only thing left to do is to inject a source at the duct entrance, which consists in forcing a potential distribution on the chosen basis. However, the only known wave is the outgoing one generated by the acoustic source, noted ϕ_+. If no reflection is expected inside the duct, this can be the value kept for the imposed potential ϕ_n. Nevertheless, apart from rare cases, there are always waves travelling in the opposite direction, noted ϕ_-, due to geometrical or flow reflections.
Let us define the reflection matrix $\mathscr{R}$ such as $\phi_- = \mathscr{R}\phi_+$. To obtain the reflection matrix $\mathscr{R}$ from the calculated admittance matrix Y, the acoustic potential and its derivative are decomposed at the entry into a right and left propagating wave as:

$$\phi_n = \phi_+ + \phi_- \text{ and } q_n = q_+ + q_-. \tag{13}$$

Using the computed admittance at the entrance and continuity conditions for the acoustic potential field and its axial derivative, the following relation is obtained:

$$Y(\phi_+ + \phi_-) = Y_+ \phi_+ + Y_- \phi_-, \tag{14}$$

with $Y_{+/-}$ corresponding to the admittance matrix associated to the waves propagating forwards or backwards at the entrance. Since the previous relation is true for any injected field ϕ_+, we obtain $\mathscr{R} = (Y - Y_-)^{-1}(Y_+ - Y)$ and the forced potential is $(I_n + \mathscr{R})\phi_+$, with I_n the identity matrix.
Finally, using equation (7), the potential field inside the whole duct is obtained as the solution of:

$$\frac{\mathrm{d}\phi_n}{\mathrm{d}x} = \left(\mathscr{A}_{11}^{-1}\mathscr{M}_{11} + \mathscr{A}_{11}^{-1}\mathscr{M}_{12}Y\right)\phi_n. \tag{15}$$

2.5 Transverse mode basis

In most multimodal studies [10, 11, 12, 19], standard basis functions are used, composed of local transverse eigenmodes ϕ_n. However, no analytical formulation of the transverse modes exists for distorted flows. These eigenmodes could be calculated at each axial section by solving a transverse eigenvalue problem, implying important calculation resources. There would then be no interest in using a multimodal formulation instead of a two-way step calculation.
Therfore, in this study, a Fourier decomposition is done in the azimuthal direction since Astley *et al.* [4] showed that the distorted modes could be represented with a limited number of azimuthal Fourier functions. In the radial direction, all the variables are projected on Chebyshev polynomials, as done previously for a multimodal formulation with a simplified flow [15]. These polynomials allow representing the boundary condition correctly and have excellent convergence properties.
Considering this, at each basis function index j, we associated a couple $(m,p) \in (\mathbb{Z},\mathbb{N})$ such that $\varphi_j = \varphi_p^m = T_p\left(\frac{r-R_1}{R_2-R_1}\right)e^{-im\theta}$, with T_p the shifted Chebyshev polynomial of the first kind of order p and m the azimuthal wavenumber.

3. Study of the acoustic propagation inside a real geometry with a distorted flow

3.1 Definition of test cases

In the following, the nacelle of the NOVA Onera airplane (side nacelle configuration) is considered [20]. For confidentiality reasons, the spatial dimensions are normalized by the fan radius and velocities by the free-stream velocity. This nacelle is placed inside a mean flow with varying free-stream velocities and an extreme angle of attack of 15 deg to study the impact of distortion.
The acoustic test cases will be performed at a frequency representative of the blade passing frequency (BPF) and for an injected mode $(m,n) = (12,1)$, with m the azimuthal wavenumber and n the radial wavenumber. This mode is cut-on for all the considered mean flow, and therefore few impacts of the distortion on the acoustic power are expected.
Baseline cases with an axisymmetric flow obtained by azimuthal averaging of the distorted flow are also performed to understand the improvement brought by the inclusion of the distortion in the acoustic model.

3.2 Mean flow computations

In this study, the mean flow is computed using Onera's CFD solver *elsA*, based on a cell-centred finite volume approach on multi-block structured meshes [21]. For this purpose, the solver is turned into a RANS mode using an implicit pseudo-time marching method with a backward Euler scheme and a second-order Jameson scheme in space. The Spalart-Allmaras model deals with the turbulence closure. For computational reasons, the fan is not simulated. The flow is driven by all external boundaries. The domain comprises around 25 million points and the simulations are run over 84 processors and last approximately ten hours.
Three cases are performed with the nacelle placed under an incidence of 15° at different free stream Mach number values M_∞. A quick overview of computed mean flow axial velocity contours provided by the CFD solver at the inlet of the duct is given in figure 2. The azimuthal inhomogeneity is visible in all cases. We observe that the nacelle behaves like an airfoil under incidence, accelerating the flow over the upper lip of the bottom part of the nacelle, and decelerating it over the lower lip of the upper part of the nacelle. This causes a difference in velocity between the upper and lower parts of the nacelle, which is responsible for the inflow distortion. Note that the flow is not completely realistic here since no fan was placed in the nacelle. In particular, the two main consequences are

that the flow velocities inside the nacelle are moderated, and extremely high inflow distortion levels are obtained. Nevertheless, for the performed acoustic study, this should not be problematic.

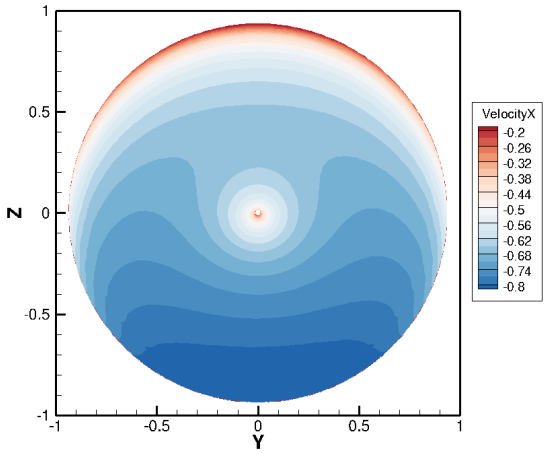

(a) $M_\infty = -0.2$

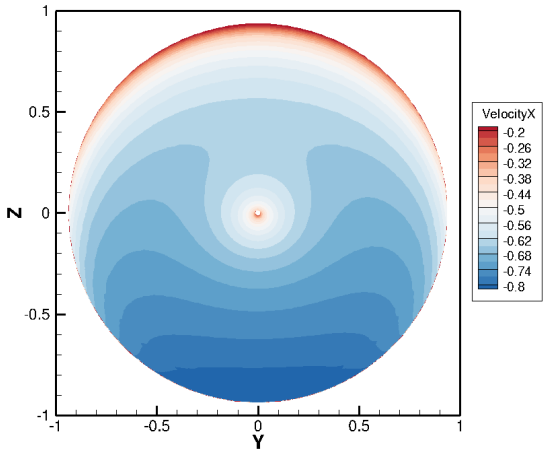

(b) $M_\infty = -0.4$

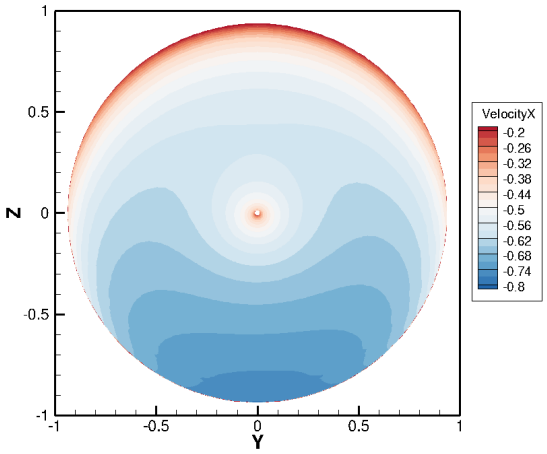

(c) $M_\infty = -0.6$

Figure 2 – Normalized axial velocity contours at the duct inlet.

For the three cases, an angular Fourier transform is performed from the axial velocity maps to get the amplitude of the distortion harmonics. The inflow distortion is also analyzed by computing the axial evolution of the circumferential distortion coefficient (CDC) applied to the axial velocity at different channel heights. This coefficient is defined as:

$$\mathrm{CDC}(x,r) = \frac{\max_\theta(U(x,r,\theta)) - \min_\theta(U(x,r,\theta))}{\mathrm{mean}_\theta(U(x,r,\theta))}. \tag{16}$$

The associated results are plotted in figure 3. It can be seen that the distortion decreases along the duct and that the CDC tends to be independent of the free stream Mach number. However, this decrease depends on the channel height, and the closer to the tip, the higher the attenuation. Near the tip, an exponential decrease is obtained. It also appears that the flow can be represented by a Fourier superposition of low order azimuthal components. Considering only the first two Fourier components for most test cases should be enough to represent the flow correctly. However, this tends to be less true as the Mach number increases.

Now that the main characteristics of the flow have been presented, let us check that the potential flow hypothesis made for developing our acoustic formulation is realistic. The vorticity magnitude

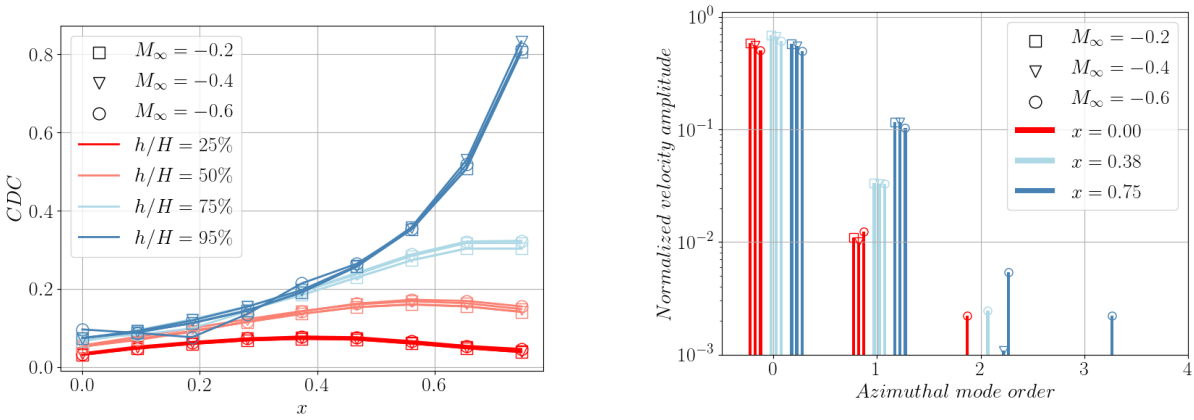

(a) Axial evolution of CDC

(b) Azimuthal Fourier transform harmonics of axial velocity at 95% of channel height

Figure 3 – Evolution of the azimuthal distortion inside the duct.

computed by the CFD solver is given at the fan and exit planes for all cases in figure 4. The vorticity magnitude is small almost everywhere compared to the distortion levels, and the potential hypothesis is reasonably respected. This hypothesis is not met inside boundary layers, but they are not included in the acoustic propagation model (perfect gas). Note that some non-physical vorticity appears on the mesh junctions (plotted in black) and is caused by numerical interpolations.

3.3 Validation of the method against a mature CAA solver

The method is validated for the case with the free-stream Mach number $M_\infty = -0.2$ against a CAA solver that does not make the potential flow hypothesis. The solver chosen is the Onera's in-house code *sAbrinA* [22, 23, 24]. It solves through finite differences the linearized Euler perturbations equation in the time domain on a structured multi-block grid. In order to dissipate the waves at the output of the domain and to avoid numerical reflected waves, an extrusion is made. The flow in that region is duplicated from the last slice of the domain. The domain comprises around 2.1 million points and the simulation is run over 168 processors and lasts approximately fifteen hours to get a converged solution.

The present multimodal method is used with twenty Chebyshev polynomials, nine azimuthal Fourier modes and a hundred points in the axial direction. The test case takes less than one minute to run with these considerations.

Iso-pressure contour plots on two axial slices (at the fan and the exit planes) and on the vertical slice $Y = 0$ are given in figures 5 and 6. The distortion impact is visible on the exit axial slice where the mode is not represented by a perfect single Fourier component in the azimuthal direction. Nevertheless, it has retained its original shape with the number of azimuthal lobes equal to the number of lobes at the injection plane. The vertical slice shows that both solutions agree that an important reflection happened with the presence of interaction lobes on the absolute pressure. As expected, it can also be noted that the iso-pressure is not symmetric around $x = 0$.

The information brought by the iso-pressure maps comparison is limited because there is little azimuthal scattering. A more quantitative comparison is thus performed by doing an azimuthal Fourier decomposition at 95% of the nacelle height for all the axial positions. The results of this projection are given in figure 7. The projection is limited to the first azimuthal neighbour modes. A relatively good agreement is obtain between both methods. The values slightly differ near the exit, but the authors observed a non-physical reflection in the CAA simulations at that level. Nevertheless, the model correctly captures the order of magnitude of the scattered waves and the reflection on the injected mode $m = 12$.

These graphs confirm that the method gives consistent results and that it can therefore be used to study the impact of distortion.

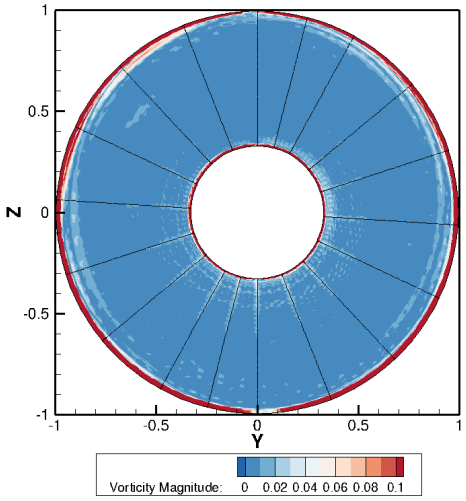

(a) Fan level. $M_\infty = -0.2$.

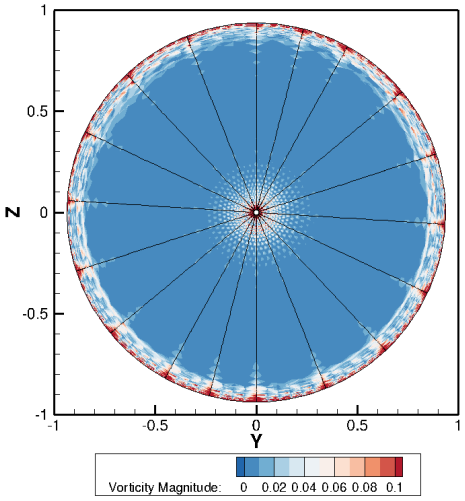

(b) Exit level. $M_\infty = -0.2$.

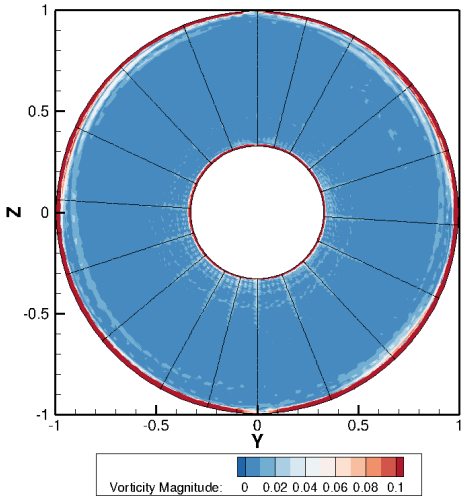

(c) Fan level. $M_\infty = -0.4$.

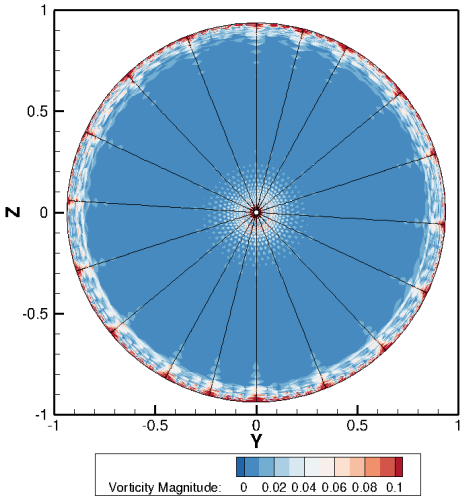

(d) Exit level. $M_\infty = -0.4$.

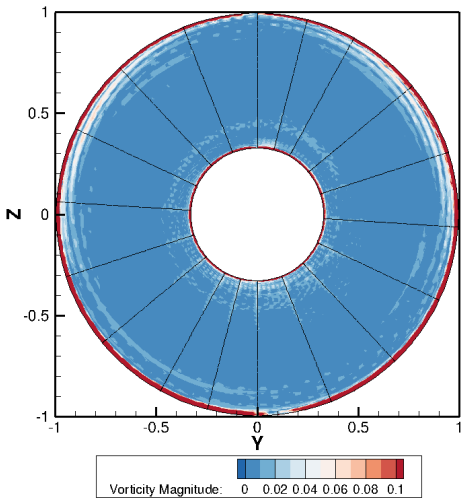

(e) Fan level. $M_\infty = -0.6$.

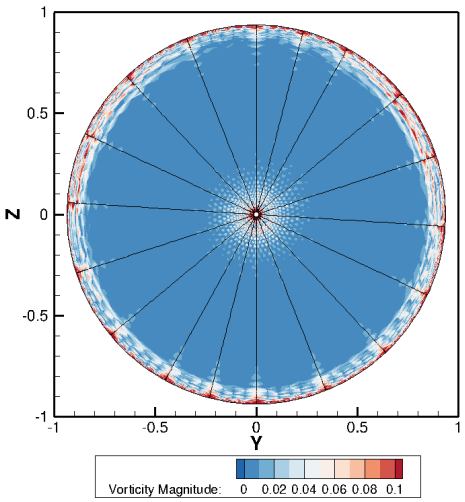

(f) Exit level. $M_\infty = -0.6$.

Figure 4 – Normalized vorticity magnitude.

3.4 Acoustic parameter study

Now that the method is shown to give consistent results, it is used to study the impact of the distortion on the propagation by comparing the results of the three different flow conditions.

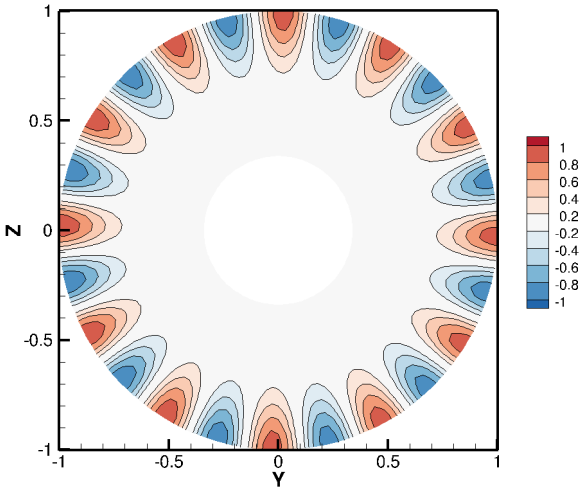

(a) Fan level. *sAbrinA*.

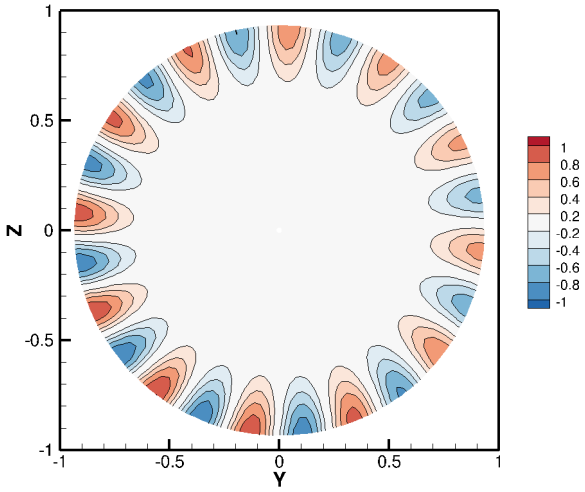

(b) Exit level. *sAbrinA*.

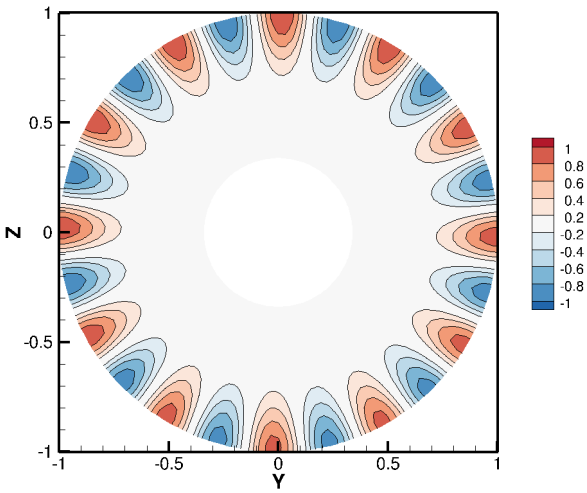

(c) Fan level. Multimodal.

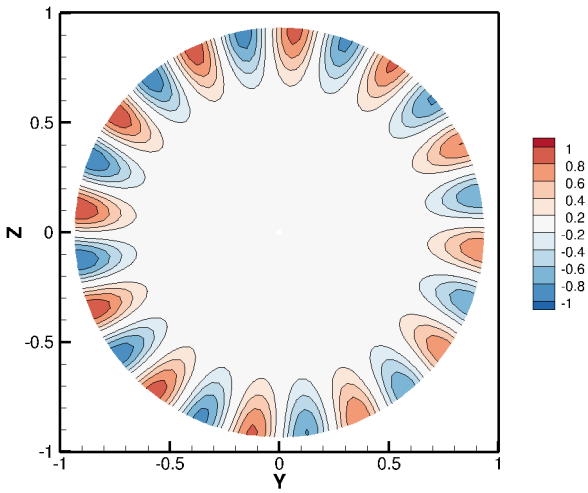

(d) Exit level. Multimodal.

Figure 5 – 2D real pressure map with an infinite Mach number $M_\infty = -0.2$.

For all the test cases, an azimuthal Fourier decomposition at 95% of the nacelle height is given at the fan and the exit planes in figure 8. In order to have a more quantitative evaluation of the distortion impact, the acoustic power is computed and compared to the baseline case (no-distortion). The associated results are given in table 1.

The first observation made is the same as the one given by Guérin *et al.*, with a decrease of the injected mode amplitude during its propagation inside the duct compared to the baseline case [7]. At the injection plane, non-injected modes are present, which shows that the distortion tends to create reflected scatter waves on azimuthal neighbours. It can also be noted that the impact of distortion is mainly seen on the direct azimuthal neighbours of the injected mode, with a scattering happening in cascade. However, the scattering is not symmetric on $m \pm k$ (with k an integer) contrarily to what was obtained inside a constant thin annular duct [7]. The mean flow also plays a key role with a scattering that is more pronounced for higher Mach numbers for a given angle of incidence (and therefore, distortion coefficient).

However, the impact of the distortion on the power level is not significant for the computed test cases, with only a minor decrease of the power levels. Note that the mode is cut-on and experiences low levels of radial scattering, which mainly explains these results. In theory, the scattered reflected waves

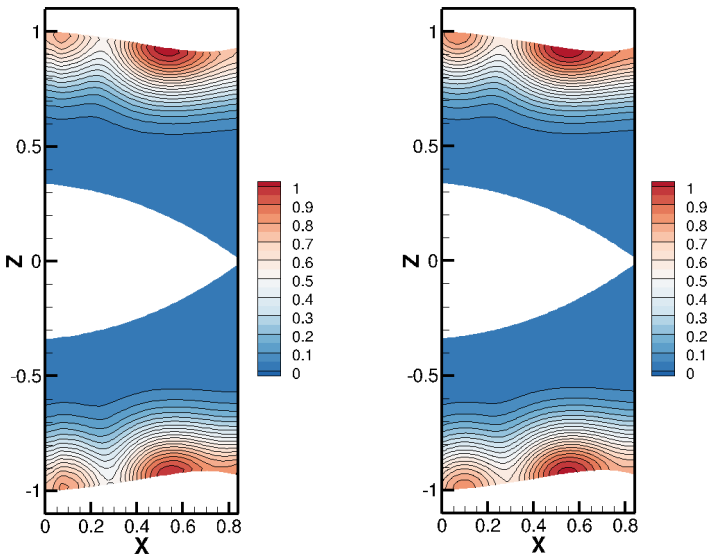

(a) *sAbrinA*. (b) Multimodal.

Figure 6 – Maps of absolute pressure on the vertical slice $Y = 0$ with an infinite Mach number $M_\infty = -0.2$.

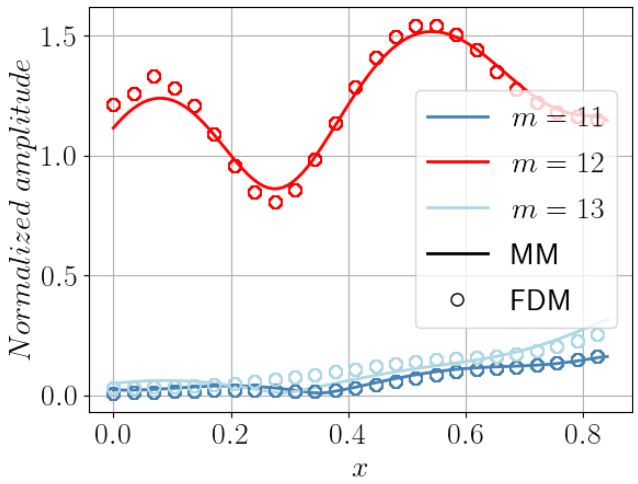

Figure 7 – Axial evolution of the azimuthal contributions to the mode at the outer wall.

could interact with other reflection phenomena (for example turning points) to form destructive or constructive interference. The conclusion on the power levels would then tend to become erroneous, but this should only happen in rare cases and that have not been observed here.
The interest in considering the distortion inside the engine is limited regarding the power levels for cut-on modes. However, the angular mode spectra show that the acoustic shape in the azimuthal direction is highly modified. Therefore the distortion would mainly impact the directivity of the field radiated outside the engine.

4. Conclusion

This paper presents a study on the acoustic propagation inside a turbofan engine with flow distortion. A multimodal method has been developed to compute the propagation of the acoustic modes in such cases. It is based on the hypothesis that the flow remains potential, which allows separating the hydrodynamic convection and the acoustic propagation. The method uses a basis of Fourier components and Chebyshev polynomials, which allows for extremely fast calculations. The speed of

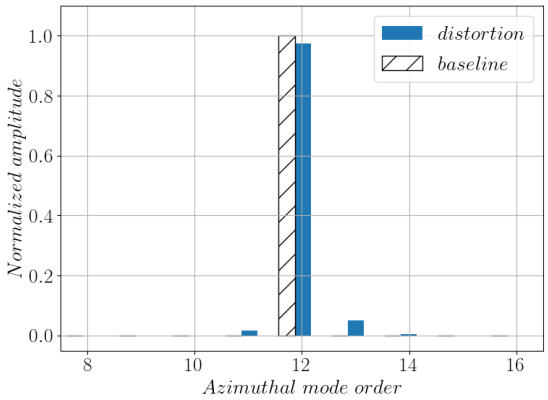

(a) Fan level. $M_\infty = -0.2$.

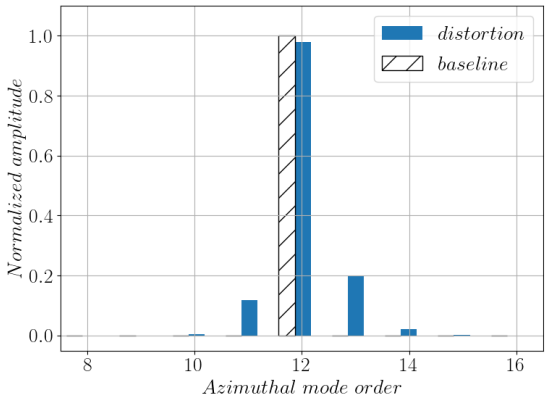

(b) Exit level. $M_\infty = -0.2$.

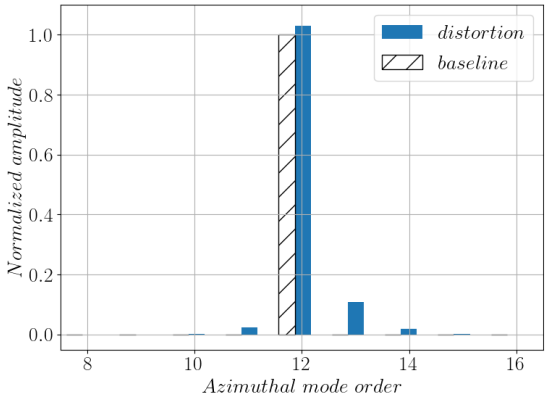

(c) Fan level. $M_\infty = -0.4$.

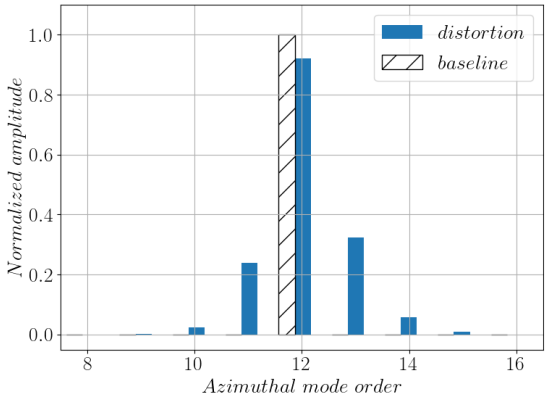

(d) Exit level. $M_\infty = -0.4$.

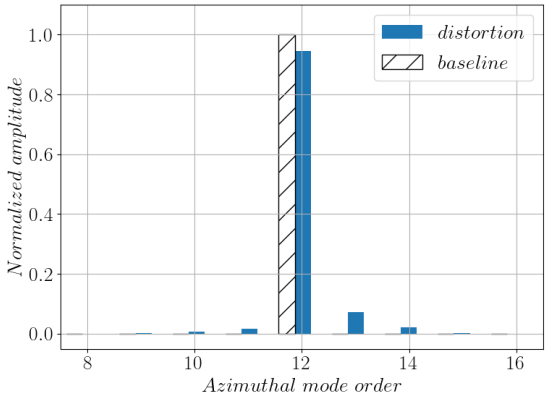

(e) Fan level. $M_\infty = -0.6$.

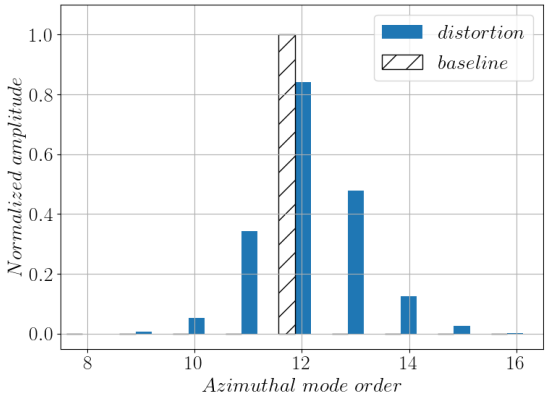

(f) Exit level. $M_\infty = -0.6$.

Figure 8 – Azimuthal decomposition of the pressure field at the outer wall (normalized by the baseline amplitude).

the method comes from the fact that the privileged propagation direction and transverse resolution are dissociated.

The method has been evaluated on the nacelle of the NOVA Onera airplane. The base flow has been obtained by performing CFD computation at various infinite Mach numbers and an extreme angle of incidence of $15°$. These simulations showed that the potential hypothesis is met outside the boundary layers. They also gave three results of main interest: the distortion levels tend to decrease sharply inside the engine, the distortion intensity is independent of the infinite Mach number, and the mean flow can be decomposed on a limited number of azimuthal components. This last observation allowed us to limit the number of Fourier coefficients used for the acoustic resolution.

Mach number	Baseline power	Distortion Power
-0.2	126.6 dB	126.5 dB
-0.4	125.9 dB	125.6 dB
-0.5	124.8 dB	124.4 dB

Table 1 – Power levels in the intake for the cut-on cases.

The developed multimodal method has been validated against a mature CAA solver. Even if the flow is not perfectly irrotational, the method correctly approximates the real acoustic field. It is, therefore, a useful tool for studying the distortion impact on the acoustic field.
The different flow cases have therefore been investigated. They have shown that the distortion does not impact significantly the induct acoustic power, and that the main effect is on the transverse shape of the mode. The amplitude of the injected Fourier mode tends to decrease, while the one of its neighbours increases. This effect is more and more pronounced as the Mach number increases. These last observations show that it would be of main interest to chain the method with a radiation tool to assess the impact of distortion on the sound directivity.

Acknowledgments

BM and MD carried out these activities in the framework of the ADEC project. This project has received funding from the Clean Sky 2 Joint Undertaking within the European Union's Horizon 2020 research and innovation program, under grant agreement GA ID No. 945583 - LPA IADP 2020-2021.

Copyright Statement

References

[1] M. Daroukh. *Effects of distortion on modern turbofan tonal noise*. PhD thesis, Institut National Polytechnique de Toulouse - Université de Sherbrooke, 2017.

[2] M. E. Goldstein. *Aeroacoustics*. McGraw-Hill International Book Company, 1976.

[3] T.G. Sofrin and D.E. Cicon. Ducted Fan Noise Propagation in Non-Uniform Flow- Part I: Test Background and Simplified Model. In *AIM 11 th Aeroacoustics Conference*, 1987.

[4] R. J. Astley, R. Sugimoto, G. Gabard, E. Norde, E. J. Grift, and Marc Bocquier. The effect of steady flow distortion on mode propagation in a turbofan intake. In *20th AIAA/CEAS Aeroacoustics Conference*, 2014.

[5] A.G. Wilson. Propagation of acoustic perturbations in non-uniform ducts with non-uniform mean flow using eigen analysis in general curvilinear coordinate systems. *Journal of Sound and Vibration*, 443:605–636, 2019.

[6] M. Daroukh, C. Polacsek, and A. Chelius. Shock wave generation and radiation from a turbofan engine under flow distortion. *AIAA Journal*, 58(2):787–801, 2020.

[7] S. Guérin, M. Vogt, and A. Holewa. Multiple scattering of acoustic waves in potential mean flow with circumferential distortion. *23rd AIAA/CEAS Aeroacoustics Conference, 2017*, (June):1–14, 2017.

[8] M. C. Duta and M. B. Giles. A three-dimensional hybrid finite element/spectral analysis of noise radiation from turbofan inlets. *Journal of Sound and Vibration*, 296(3):623–642, 2006.

[9] A. G. Prinn, R. Sugimoto, and R. J. Astley. The effect of steady flow distortion on noise propagation in turbofan intakes. *22nd AIAA/CEAS Aeroacoustics Conference, 2016*, pages 1–14, 2016.

[10] V. Pagneux, N. Amir, and J. Kergomard. A study of wave propagation in varying cross-section waveguides

by modal decomposition. Part I. Theory and validation. *The Journal of the Acoustical Society of America*, 100(4):2034, 1996.

[11] S. Félix and V. Pagneux. Multimodal analysis of acoustic propagation in three-dimensional bends. *Wave Motion*, 36(2):157–168, 2002.

[12] V. Pagneux. Multimodal admittance method in waveguides and singularity behavior at high frequencies. *Journal of Computational and Applied Mathematics*, 234(6):1834–1841, 2010.

[13] S. Félix, J. B. Doc, and M. Boucher. Modeling of the multimodal radiation from an open-ended waveguide. *The Journal of the Acoustical Society of America*, 143(6):3520–3528, 2018.

[14] T. Guennoc, J. B. Doc, and S. Félix. Improved multimodal formulation of the wave propagation in a 3D waveguide with varying cross-section and curvature. *The Journal of the Acoustical Society of America*, 149(1):476–486, 2021.

[15] B. Mangin, M. Daroukh, and G. Gabard. Propagation of acoustic waves in a slowly varying duct with multiple-scales potential flow using the multimodal formulation. In *28nd AIAA/CEAS Aeroacoustics Conference*, 2022.

[16] A. J. Cooper and N. Peake. Propagation of unsteady disturbances in a slowly varying duct with mean swirling flow. *Journal of Fluid Mechanics*, 445:207–234, 2001.

[17] Ya Yan Lu. A fourth-order Magnus scheme for Helmholtz equation. *Journal of Computational and Applied Mathematics*, 173(2):247–258, 2005.

[18] E. Redon, A. S. B. B. Dhia, J. F. Mercier, and S. P. Sari. Non-reflecting boundary conditions for acoustic propagation in ducts with acoustic treatment and mean flow. International Journal for Numerical Methods in Engineering. *International Journal for Numerical Methods in Engineering*, 86(11):1360–1378, 2011.

[19] James P. McTavish and Edward J. Brambley. Nonlinear sound propagation in two-dimensional curved ducts: A multimodal approach. *Journal of Fluid Mechanics*, 875:411–447, 2019.

[20] L. Wiart, O. Atinault, R. Grenon, B. Paluch, and D. Hue. Development of NOVA Aircraft Configurations for Large Engine Integration Studies. In *33rd AIAA Applied Aerodynamics Conference*, volume 2254, 2015.

[21] L. Cambier, S. Heib, and S. Plot. The Onera elsA CFD Software: Input from Research and Feedback from Industry. *Mechanics and Industry*, 14(3):159–174, 2013.

[22] S. Redonnet, E. Manoha, and P. Sagaut. Numerical simulation of propagation of small perturbations interacting with flows and solid bodies. In *7th AIAA/CEAS Aeroacoustics Conference and Exhibit*, 2001.

[23] S. Redonnet and Y. Druon. Computational aeroacoustics of aft fan noises characterizing a realistic coaxial engine. *AIAA Journal*, 50(5):1029–1046, 2012.

[24] S. Redonnet and G. Cunha. An advanced hybrid method for the acoustic prediction. *Advances in Engineering Software*, 88:30–52, 2015.